This is the preprint version of the following article:

which has been published in final form at:

Suspension of discrete microscopic oscillators as a model of an ultrasonic metafluid

Aljaž Draškovič-Bračun[1,2], Tilen Potisk[1,2], Matej Praprotnik[1,2], and Daniel Svenšek[1,2,*]

[1]*Laboratory of Molecular Modeling, National Institute of Chemistry, SI-1001 Ljubljana, Slovenia*
[2]*Department of Physics, Faculty of Mathematics and Physics, University of Ljubljana, SI-1000 Ljubljana, Slovenia*
[*]*email: daniel.svensek@fmf.uni-lj.si*
(Dated: November 23, 2022)

We present a model of ultrasonic metafluids — acoustic metamaterials in the form of suspensions of discrete microscopic oscillators coupled to the embedding fluid. Contrary to a common assumption about metamaterials, and as already established in the field of metafluids, the metafluid concept need not be based on position periodicity or correlation of the suspended micro-oscillators, and in this case not even on ideally designed micro-oscillators. For the speculation that metafluids may one day be produced as solutions of macromolecules, it is essential that the micro-oscillators be allowed to be randomly distributed in the host fluid and generally have irregular (modal) shapes. We formulate the detailed operating principle of such a metafluid model, give explicit formulae for its effective dynamic moduli in terms of the modal structure of the micro-oscillators, and discuss basic practical issues of performance optimization in terms of their mass and size.

This work builds on the fascination that suspensions of irregular, possibly macromolecular or microprinted entities that act as micro-oscillators could function as ultrasonic metamaterials in certain frequency windows.

Mechanical acoustic metamaterials [1–3] realized in practice are based on principles of waveguides with cavity and membrane resonators [4–11], perforated plates [12], coiled-up space in two- and three-dimensional labyrinths [13, 14], and various synthetic (elasto)mechanical unit cells [1, 3]. These are all artificial, elaborately constructed, spatially ordered systems that can induce negative phase velocity of airborne or structure-borne sound waves, resulting in unusual wave propagation characteristics such as negative refracion. In addition, active acoustic metamaterials with electromechanical sensing and transducing units have been realized [15–17], where any desired response of the units is driven and controlled by tailored electronic signals. Remarkably, a physiological acoustic metamaterial has also been recently reported [18] — moth wings are found to act as metamaterial ultrasound absorbers.

In soft materials, various models have been investigated, mainly theoretically, from bubbles [19–25] and elastic spheres [26–29] suspended in liquids or soft solids, periodic fluid-solid [30, 31] or hard sphere-soft matrix [32] composites. Scattering by monopolar resonances of single bubbles or pairs of bubbles has been rigorously treated in ref. [19], and a pair of spherical bubbles subject to general axisymmetric shape oscillations in ref. [33]. Acoustic metafluid with negative index over a wide frequency range around 0.1 MHz based on Mie resonances in suspended porous microbeads has been practically realized [34] and compared against multiple scattering modeling. An absorption metascreen in the form of a two-dimensional bubble array with coupled monopolar resonances has been presented both theoretically and experimentally [22, 24]. Multiple scattering by monopolar resonances of a large number of disordered bubbles was computationally modeled [23], including the dipole response for smaller bubble spacing [20].

In liquid systems, the dynamic bulk modulus is relatively easily affected by bubble- or vesicle-like inclusions. In medical ultrasound imaging, for example, such objects, e.g., encapsulated microbubbles injected into the blood stream, are specifically used as contrast agents because of their strong scattering at monopolar resonances. These contrast agents are typically 1–10 μm in diameter and comprised of a biologically inert gas, e.g, air or high molecular weight gases (perfluorocarbon, sulfur hexafluoride or nitrogen), stabilized within a lipid, protein, or polymer shell [35–38]. Creating resonances that would affect the dynamic density of the fluid, on the other hand, is a more difficult task. In order to affect the density, the inclusions must exert a force on the fluid, and therefore the corresponding resonances must have a vectorial, i.e. dipolar angular symmetry. Unlike mechanical systems supported by a structure or frame, in fluid environments there is no external reaction force on the wave-carrying medium, i.e., recoil from the structure as, e.g., in the case of membranes, is not possible. Thus, the lowest dipolar modes of the inclusions are rigid translations with zero frequency. Therefore, one must reckon with dipolar modes of higher radial order [34, 39], in which, for example, the central part of the object moves in the opposite direction to the outer regions. If the object is to effectively recoil from the embedding fluid and thus exert a force on the fluid, the central part must be hidden, i.e. effectively inaccessible to the fluid.

We should note that bubbles (unlike droplets, for example) have no such dipolar modes at all. Their undulations are completely described by an angle-dependent radial displacement from the spherical equilibrium shape and the normal modes are scalar spherical harmonics. ¿From their orthogonality it follows that there is only one dipolar mode, i.e., trivial translation with zero frequency, and only one breathing (volume-changing) mode. All higher modes are strictly volume-preserving and do not shift the center of mass of the surrounding fluid. Some elasticity of the bubble shell is additionally required to obtain higher modes with dipolar symmetry, which could,
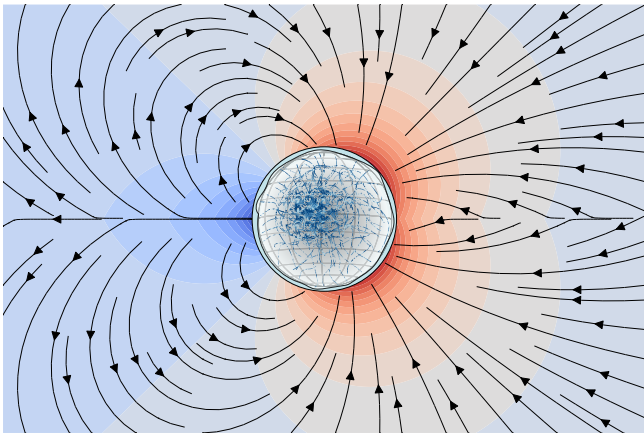
Figure 1. Schematic of a micro-oscillator working principle: a macromolecular entity is excited by the acoustic field and generates local flow (arrows) of the host fluid; the contours indicate the corresponding pressure. The dipole component of the flow is associated with a "hidden" force on the fluid. Dipolar contributions of many micro-oscillators add up to smooth flow and hidden-force fields, while contributions of the monopole component (which dominates in the long-wavelength limit and is not shown) add up to a smooth volume source field. The former change the effective density and the latter the effective compressibility of the medium experienced by the ultrasonic wave. For a continuous medium, these two effects are described by Eqs. (1) and (4), respectively.

at least in principle, shift the center of mass of the surrounding fluid.

Therefore, to avoid the need for dipolar modes, the concept of dipolar resonances of dimers arising from multiple scattering was invoked, with a very illustrative demonstration using two-dimensional lattices of soda cans as Helmholtz resonators [40]. In the case of bubbles, this effect was theoretically exploited in ref. [21], showing that multiple scattering due to monopolar resonances of disordered but positionally pair-correlated bubbles can lead to simultaneously negative values of the dynamic mass density and compressibility. However, the design of a disordered medium with pairwise spatial correlations between the monopolar resonators is a prerequisite to ensure the effectiveness of this pairwise coupling.

Higher dipolar modes that shift the center of mass of the surrounding fluid are certainly present in droplets and similar full objects with radial degrees of freedom. When excited, they represent the source of the hidden force on the fluid [39]. However, to obtain such higher modes in the objects, which should be much smaller than the wavelength in the host fluid, they must have a much lower speed of sound than the host fluid. For objects made of continuous media, this is a serious limiting factor. One way out is to use a heterogeneous, highly porous inclusions [34] in which the speed of sound can be reduced by more than an order of magnitude due to the high compressibility of the air in the pores, while maintaining the high mass density due to the skeleton.

With this work, we take a different approach and model ultrasonic metafluids in the form of suspensions of *discrete* microscopic oscillators with specific and inherently irregular modal shapes. The model oscillator, described in Sec. II, is represented by a quasi-spherical collection of point masses interacting with harmonic springs. Because of the possibility of specific and locally very different interactions between the particles in this discrete network, which do not occur in a continuum — one of these features is the topology, the coordination number of important connections between particles — the normal modes cannot be categorized in advance and are susceptible to qualitative changes resulting from changes in the local connection rules. However, the main difference from the continuum are the so-called floppy or soft modes [41–45] with unusually low frequencies, known also in semi-rigid elastic networks used in modeling proteins [43–48]. They arise from low-energy internal bond-rotational degrees of freedom that typically form in the underconstrained regions of the structure. Such anomalous floppy modes could potentially extend the lower frequency end of macromolecules, such as large proteins, into the supersonic range.

With this motivation in mind, we model the metamaterial behavior as a generic phenomenon that is not restricted to regular objects such as bubbles or elastic spheres, nor to a regular organization in the sense of a particular spatial periodicity or correlation. For a potential metafluid without fully controlled design, these aspects are essential. Moreover, modal irregularity opens up more possibilities for the realization of negative dynamic density, while preserving the convenient breathing resonances of bubbles and vesicles. Practically, such a metafluid could also consist of two components — the somewhat simpler bubble- or vesicle-like component that affects the dynamic compressibility, and another, more complex component that affects the dynamic density. Possible candidates for the latter are globular macromolecular structures such as large globular proteins, protein bubbles, multilamellar vesicles below the bilayer gel-to-liquid transition, and other microscopic structures without strong inherent damping. The possibility that some of them could even be synthesized via a biological pathway is very tantalizing. Today, microscopic oscillators with sufficient dynamic functionality could be also microprinted in large numbers to obtain an artificial acoustic suspension.

Acoustic response is not readily associated with the microscopic or even macromolecular world, and not so much with soft matter in general. The aforementioned applications of encapsulated microbubbles [35–38] in MHz-range medical ultrasound imaging show, however, that this is a real option. The scaling $\omega \propto 1/\sqrt{m}$ of molecular normal mode frequencies ω with molecular mass m suggests that sufficiently large macromolecules can exhibit acoustically relevant frequencies. Indeed, breathing mode frequencies of large proteins extend down to $\sim 1\,\mathrm{GHz}$, where the attenuation length of ultrasound in water is still about

50 µm [49] and would thus allow miniature applications.

We will comprehensively explain the concept of such metafluids and describe their principle of operation in detail. It is schematically sketched in Fig. 1. ¿From the normal modes of the micro-oscillator units coupled to the surrounding fluid, we will calculate the response of the units to acoustic excitation. We will also estimate the width of the coupled modes due to viscous damping in the fluid. All this allows us to arrive at a self-consistent continuum solution that explicitly defines the two macroscopic effective moduli — dynamic compressibility and density — that govern acoustic propagation in this meta-medium. We demonstrate that both effective moduli can indeed become negative and show when this happens. Particular attention is paid to achieving negative dynamic density, which is the main challenge with metafluids.

I. ACOUSTIC WAVE EQUATION OF A METAFLUID

The metafluid is a two-component system — a host fluid component (the main component, water), in which a micro-oscillator component is randomly distributed. We will treat it in the dilute limit, which means that the micro-oscillators do not communicate directly with each other, but only indirectly via their continuum (mean-field) pressure and flow fields. Thus, ideally, we have two separations of length scales: the micro-units are sufficiently far apart (dilute limit), while their mean distance is still small compared to the acoustic wavelength (the usual limit for a metamaterial). Note that this idealization is applicable for ultrasound in water up to about 100 MHz.

We describe the dynamics of acoustic waves in the main component, while the micro-oscillator component gives rise to "hidden" force [50, 51] and volumetric flux source. This will result in an effective wave equation for the main component with an effective dynamic density $\rho^{\text{eff}}(\omega)$ and an effective dynamic compressibility $\chi^{\text{eff}}(\omega)$.

With $e^{-i\omega t}$ as the time factor used from now on, the linearized Euler equation for the main component is

$$-i\omega\rho_0 \mathbf{u} = -\nabla p + \mathbf{f}', \tag{1}$$

where ρ_0 is the density of the main component, $\mathbf{u}$ is its acoustic (macroscopic) velocity, p is the acoustic pressure and $\mathbf{f}'$ is the hidden force density. In the view of the two component system, $-\nabla p$ is an external force on both components, while $\mathbf{f}'$ is an additional internal force of the micro-oscillator component on the main component. This separation is absolutely crucial — these two forces are physically distinct and cannot be reduced to a single quantity, i.e., the partitioning of the total force density on the main component into both contributions is not a matter of choice.

In the following part of this Section, dynamic density and compressibility moduli are justified and systemati-

cally introduced. Readers familiar with the subject may proceed directly to Section II.

The hidden force arises from the oscillation of the micro-oscillators excited by the acoustic field, i.e., by the local acoustic pressure or velocity or both, depending on the coupling mechanism (pressure or viscous drive). Importantly, in a linear system, the excited amplitude is linear in the amplitudes of the acoustic fields p and $\mathbf{u}$ (which are themselves linearly related) and the resulting force $\mathbf{F}_1$ of a single micro-oscillator on the fluid is also linear in the excited amplitude of the micro-oscillator. Therefore, in the homogeneous limit the hidden force density $\mathbf{f}' = \rho_N \mathbf{F}_1$ of the micro-oscillators with number density ρ_N can be written in the form

$$\mathbf{f}' \equiv i\omega\rho'(\omega)\mathbf{u}, \tag{2}$$

with $\rho' \propto \rho_N$. Eq. (1) then becomes

$$-i\omega\left[\rho_0 + \rho'(\omega)\right]\mathbf{u} = -\nabla p, \tag{3}$$

where $\rho^{\text{eff}} \equiv \rho_0 + \rho'(\omega)$ is an effective dynamic density of the metafluid.

The continuity equation for the main component, with $d\rho_0/\rho_0 = \chi_0 dp$ the equation of state of the main component and χ_0 its compressibility, is in the usual linearized form

$$-i\omega\chi_0 p + \nabla \cdot \mathbf{u} = q', \tag{4}$$

where q' is the additional, hidden volume source density (volume flux per unit volume) due to the breathing oscillations of the micro-oscillator component. Again, the volume source Q_1 of a single micro-oscillator is linear in its excited amplitude and thus linear in p, such that in the homogeneous limit the hidden volume source density $q' = \rho_N Q_1$ can be written in the form

$$q' \equiv i\omega\chi'(\omega)p, \tag{5}$$

with $\chi' \propto \rho_N$. Eq. (4) then becomes

$$-i\omega\left[\chi_0 + \chi'(\omega)\right]p = -\nabla \cdot \mathbf{u}, \tag{6}$$

where $\chi^{\text{eff}} \equiv \chi_0 + \chi'(\omega)$ is an effective dynamic compressibility of the metafluid.

Finally, from Eqs. (3) and (6) follows the acoustic wave equation of the metafluid,

$$\nabla^2 p + \omega^2 \chi^{\text{eff}}(\omega)\rho^{\text{eff}}(\omega)\, p = 0, \tag{7}$$

where $\chi^{\text{eff}}\rho^{\text{eff}} = 1/c^2$ defines the speed of sound c in the metafluid. The particularly interesting case of the double negative metafluid occurs at frequencies where both $\chi^{\text{eff}}(\omega)$ and $\rho^{\text{eff}}(\omega)$ are negative and thus c^2 is real.

In Secs. IV and V, we will determine the effective moduli ρ^{eff} and χ^{eff} from the modal structure of the micro-oscillator. In Sec. II, we must first determine these eigenmodes, taking into account the coupling with the surrounding fluid, which introduces a nontrivial additional mass load.

II. FLUID-COUPLED MICRO-OSCILLATOR

The micro-oscillator unit is generically represented by a discrete globular, quasi-spherical ensemble of point masses m_i with harmonic expansion

$$U_{ij} = \frac{1}{2} k_{ij} \left[\hat{\mathbf{e}}_{ij} \cdot (\mathbf{x}_i - \mathbf{x}_j)\right]^2, \quad \hat{\mathbf{e}}_{ij} \equiv \frac{\mathbf{R}_i - \mathbf{R}_j}{|\mathbf{R}_i - \mathbf{R}_j|}, \quad (8)$$

of their distance-dependent quadratic pair potentials $U_{ij} = \frac{1}{2} k_{ij}(|\mathbf{R}_i + \mathbf{x}_i - \mathbf{R}_j - \mathbf{x}_j| - |\mathbf{R}_i - \mathbf{R}_j|)^2$ with force constants k_{ij}, where $\mathbf{R}_i$ is the equilibrium position of i-th particle and $\mathbf{x}_i$ its fluctuation. Such a generic discrete approach in the spirit of anisotropic network models [44, 46, 47] of proteins is convenient, since practically any microscopic system can be modeled in this sense and then always coupled to the surrounding fluid in the same manner.

In the present study, we couple the dynamics of the micro-oscillator with the surrounding host fluid by considering incompressible irrotational (potential) flow of the fluid and neglecting its viscosity η. The inviscid approximation is typical of an acoustic medium that is sufficiently transparent to sound waves, while the incompressibility assumption corresponds to the omission of the radiation pressure applicable in the long-wavelength limit.

To ensure that the viscous effects are small even for the microscopic flow field $\mathbf{v}$ around the micro-oscillator and the potential flow assumption is sufficient, the radius r_0 of the micro-oscillator should not be too small. The requirement that the inertial forces dominate over the viscous ones, $\rho_0 \omega v \gg \eta \nabla^2 v$, leads to the condition $r_0 \gg \sqrt{2\eta/(\rho_0 \omega)}$, i.e., the micro-oscillator must be large compared to the penetration length of oscillatory shear ($\sim 0.18\,\mu\text{m}$ for ultrasound with frequency $\nu \sim 10\,\text{MHz}$ in water).

The values of the parameters are selected according to the following strategy. The mean density of the micro-oscillator is kept on the order of ρ_0, which is also confirmed by the results as the relevant density scale. This sets the mass of the micro-oscillator given its typical micron size. Finally, the constants k_{ij} are chosen such that the relevant resonances occur at frequencies in the typical ultrasonic range of $10\,\text{MHz}$, which is also realistic for micron-sized objects.

To ensure strong coupling of the micro-oscillator to the surrounding fluid, it is assumed that the surface of the micro-oscillator is impermeable to the fluid. In practice, this may be a physical surface due to hydrophobicity, as in the case of a lipid bilayer, or an effective surface defined by a depletion layer. It is essential that the modeled contact surface with the fluid, albeit discrete, is complete and that pressure forces acting on it are described exactly. Otherwise a homogeneous pressure field will lead to a spurious net force on the micro-oscillator, which in the long-wavelength limit will prevail over actual pressure gradient force. Therefore, the interfacial part of the mesh is triangulated and the pressure force $\mathbf{F}^{\triangle}$ on each triangle is distributed to its three vertices A, B, C by the requirement of zero in-plane torque on the triangle,

$$\mathbf{F}_A = \mathbf{F}_B = \mathbf{F}_C = \mathbf{F}^{\triangle}/3. \quad (9)$$

Similarly, the velocity of the triangle's center is expressed with the velocities of the vertices as

$$\mathbf{v}^{\triangle} = (\mathbf{v}_A + \mathbf{v}_B + \mathbf{v}_C)/3. \quad (10)$$

The velocity potential of the surrounding fluid with velocity $\mathbf{v}(\mathbf{r})$ is of the general form

$$\Phi(r, \theta, \phi) = \sum_{lm} b_{lm} \left(\frac{r}{r_0}\right)^{-(l+1)} Y_{lm}^{\mathbb{R}}(\theta, \phi), \quad \mathbf{v} = \nabla \Phi, \quad (11)$$

where $Y_{lm}^{\mathbb{R}}$ are real combinations of spherical harmonics[1]. We will determine the multipole coefficients b_{lm} by relating the radial component $v_r(r_0, \theta, \phi) = \partial \Phi/\partial r$ of the flow velocity on a virtual sphere $r = r_0$ to the motion of the triangles. This sphere can be the average effective surface of the micro-oscillator, or its circumscribed sphere as illustrated in Fig. 1. In our examples, all surface points will lie on this sphere, but this is not necessary in general. By integrating over the sphere and considering the orthogonality of $Y_{lm}^{\mathbb{R}}$,

$$b_{lm} = -\frac{1}{l+1} \frac{1}{r_0} \int dS\, v_r(r_0, \theta, \phi)\, Y_{lm}^{\mathbb{R}}(\theta, \phi). \quad (12)$$

The knowledge of the continuous function $v_r(r_0, \theta, \phi)$ is required. In the simplest discrete approximation, we replace the integral by a sum over the triangles $\triangle^j$, that is $\sum_{\triangle^j} S^j v_r(r_0, \theta^{\triangle^j}, \phi^{\triangle^j}) Y_{lm}^{\mathbb{R}}(\theta^{\triangle^j}, \phi^{\triangle^j})$, where the superscript $\triangle^j$ denotes the values at the centers of the triangles and S^j are their areas.

The single scalar boundary condition for potential flow requires that the normal velocity of the center of the triangle (i.e., the average normal velocity of the triangle) be equal to the normal velocity of the fluid at that point (whereas any rotation of the triangle about an axis through its center is coupled only to the rotational components of the flow). Stating this normal boundary condition for the radial velocity components in Eq. (12) is a convenient approximation. Then, with respect to outward normals $\hat{\mathbf{n}}^j$ of the triangles, we obtain

$$b_{lm} = -\frac{1}{l+1} \frac{1}{r_0} \sum_{\triangle^j} S^j \left[\left(\mathbf{v}^{\triangle^j} \cdot \hat{\mathbf{n}}^j\right) \hat{\mathbf{n}}^j\right] \cdot \hat{\mathbf{e}}_r^{\triangle^j} Y_{lm}^{\mathbb{R}\triangle^j}, \quad (13)$$

where $\hat{\mathbf{e}}_r^{\triangle^j}$ are radial directions at the centers of the triangles and $S^j \hat{\mathbf{n}}^j \cdot \hat{\mathbf{e}}_r^{\triangle^j}$ are radial projections of their faces.

---

[1] A Green's function boundary element formulation [52] is an alternative. Here, the spherical harmonics expansion is preferred, mainly because of the tractability of the dissipation integrals, Appendix A.

We thus see that in this approximation the coefficients b_{lm} of the potential flow Eq. (11) are expressed by the volume fluxes through the virtual sphere $r = r_0$ generated by the normal translation of the triangles.

In Eq. (13), only the midpoint values of the spherical harmonics are used instead of their complicated integrals over the triangles. Thus, when l in Eq. (11) is brought to high values, one gets sharper and sharper peaks of $\Phi(r_0, \theta, \phi)$ as the series reproduces this discrete function more and more accurately. To avoid this artifact, it is necessary to truncate the series at $l = l_{max}$ such that the number of terms $(l_{max}+1)^2$, i.e., the number of degrees of freedom, is of the order of the number of surface points.

Taking into account the linearized form of the Bernoulli equation, $p = -\rho_0 \partial \Phi / \partial t$, i.e.,

$$p = \mathrm{i}\omega\rho_0\Phi, \tag{14}$$

the pressure force on a triangle, resulting from the flow Eq. (11) of the surrounding fluid, is $\mathbf{F}^{\triangle^i} = S^i(-\hat{\mathbf{n}}^i)p^{\triangle^i} = -\mathrm{i}\omega\rho_0 S^i\hat{\mathbf{n}}^i\Phi^{\triangle^i}$. In agreement with the radial direction approximation assumed in Eq. (13), it turns out, however, that we must again introduce a radial projection,

$$\mathbf{F}^{\triangle^i} = -\mathrm{i}\omega\rho_0 S^i\hat{\mathbf{n}}^i\left(\hat{\mathbf{n}}^i \cdot \hat{\mathbf{e}}_r^{\triangle^i}\right)\Phi^{\triangle^i}, \tag{15}$$

which can be interpreted as the normal component of the pressure force acting on the spherical cap belonging to the triangle. Inserting the expressions Eqs. (11) and (13),

$$\mathbf{F}^{\triangle^i} = \frac{\omega^2\rho_0}{r_0}S^i\hat{\mathbf{n}}^i\left(\hat{\mathbf{n}}^i \cdot \hat{\mathbf{e}}_r^{\triangle^i}\right) \times \tag{16}$$
$$\times \sum_{lm}\frac{1}{l+1}\sum_{\triangle^j}S^j\left(\hat{\mathbf{n}}^j \cdot \hat{\mathbf{e}}_r^{\triangle^j}\right)\left(\hat{\mathbf{n}}^j \cdot \mathbf{x}^{\triangle^j}\right)Y_{lm}^{\mathbb{R}\triangle^j}Y_{lm}^{\mathbb{R}\triangle^i},$$

we obtain a closed expression for the force $\mathbf{F}^{\triangle^i}$ on a triangle i in terms of a linear combination of displacements $\mathbf{x}^{\triangle^j}$ of centers of all triangles j. Importantly, the radial projection in Eq. (15) ensures that in Eq. (16) the coefficient of $\mathbf{x}^{\triangle^j}$ appearing in $\mathbf{F}^{\triangle^i}$ and the coefficient of $\mathbf{x}^{\triangle^i}$ appearing in $\mathbf{F}^{\triangle^j}$ are identical and hence the effective mass matrix in Eq. (19) will be symmetric.

We can now write down Newton's law for a particle i,

$$-m_i\omega^2\mathbf{x}_i = -\sum_j\frac{\mathrm{d}U_{ij}}{\mathrm{d}\mathbf{x}_i} + \mathbf{F}_i^p, \tag{17}$$

where the pressure force

$$\mathbf{F}_i^p = \frac{1}{3}\sum_{\triangle^k \ni i}\mathbf{F}^{\triangle^k} \tag{18}$$

is nonzero for the particles on the surface of the micro-oscillator and is obtained by adding contributions Eq. (16) of all triangles with vertex i, considering the simple connections Eqs. (9) and (10).

In a clean matrix form for the "supervector" $\mathbf{x} = \{\mathbf{x}_i\}$ of the particle vectors $\mathbf{x}_i$, Eq. (17) becomes

$$-\omega^2\mathsf{T}\mathbf{x} = -\mathsf{V}\mathbf{x}, \tag{19}$$

where V is the interparticle force matrix defined by the quadratic pair potentials Eq. (8), which is symmetric by definition, and $\mathsf{T} \equiv \mathsf{M} + \mathsf{A}$ is the effective mass matrix of the fluid-coupled micro-oscillator, with M the trivial diagonal matrix of the point masses m_i and A the additional effective mass matrix due to the fluid. The matrix A results from Eqs. (16), (10) and (18), and is a full, symmetric matrix. The latter is ensured by the analogous projections in Eqs. (13) and (15).

We can check a simple limit — that of a symmetric breathing mode of a perfect sphere with amplitude Δr_0. For this spherically symmetric velocity $v_r = -\mathrm{i}\omega\Delta r_0$ of the sphere surface, Eq. (12) yields the only nonzero coefficient $b_{00} = \sqrt{4\pi}\mathrm{i}\omega r_0\Delta r_0$, the velocity potential Eq. (11) is then $\Phi(r) = \mathrm{i}\omega r_0(r_0/r)\Delta r_0$ and the fluid pressure Eq. (14) at the sphere surface is

$$p = -\omega^2\rho_0 r_0\Delta r_0. \tag{20}$$

In passing, the fluid pressure can also be written in terms of an effective mass load m_{fluid} of the fluid, $p = -m_{\text{fluid}}\,\omega^2/(4\pi r_0^2)$, which is thus three times the fluid mass m_0 displaced by the sphere,

$$m_{\text{fluid}} = 3m_0. \tag{21}$$

Balancing the fluid pressure Eq. (20) and the pressure $p = -3\chi^{-1}\Delta r_0/r_0$ inside the bubble, where χ is the compressibility of the bubble, the natural (Minnaert [53]) frequency of a bubble entrapped in the fluid is $\omega = \sqrt{3/(\rho_0\chi)}/r_0$.

A. Coupled modes

For symmetric matrices T and V, the generalized eigensystem Eq. (19) is solved by eigenvectors $\mathbf{x}^i$ (denoted by the superscript),

$$\mathsf{V}\mathbf{x}^i = \omega_i^2\mathsf{T}\mathbf{x}^i, \quad \mathbf{x}^j\mathsf{T}\mathbf{x}^i = 0 \iff \omega_i^2 \neq \omega_j^2, \tag{22}$$

which are, for different eigenvalues ω_i^2, orthogonal with respect to the scalar product with T. Note that for the fluid-coupled micro-oscillator, T is a full matrix. Due to the translational and rotational symmetry of the whole system, there are 3 translational and 3 rotational degenerate modes with zero frequency. For a complete orthogonal basis, this 6-dimensional subspace (the null space of V) must be orthogonalized with respect to T. Additional degeneracies are present in the case of a symmetric (particle positions $\mathbf{R}_i$, stiffness constants k_{ij}) micro-oscillator and must be orthogonalized.

For a physical interpretation, one must keep in mind that T maps from the space of displacements $\mathbf{x}$ to the

space of forces, i.e., up to the factor ω^2, $\mathsf{T}\mathbf{x}$ is the vector of forces needed to generate the displacement vector $\mathbf{x}$ if the forces $\mathsf{V}\mathbf{x}$ between the particles were not present. So the scalar product $\mathbf{y}\mathsf{T}\mathbf{x}$ is between a displacement vector $\mathbf{y}$ and the force vector giving a displacement vector $\mathbf{x}$ for $\mathsf{V} = 0$.

III. ACOUSTIC SOLUTION AND EXCITATION OF COUPLED MODES

The dynamic equation Eq. (19) for the fluid-coupled micro-oscillator has been written in the system where the far-field fluid is at rest, i.e., the motion of the fluid is due only to the motion $\mathbf{x}$ of the micro-oscillator. In the presence of a long-wavelength acoustic wave with frequency ω and amplitude $\mathbf{a}_0$, the total solution vector of the micro-oscillator is

$$\mathbf{x}^{\text{tot}}(\omega) = \mathbf{a}^0(\omega) + \mathbf{x}(\omega), \qquad (23)$$

where $\mathbf{a}^0$ is the "supervector" of rigid translation, i.e., $\mathbf{a}_0$ for each particle. The corresponding solution in the fluid component is $\mathbf{v}(\omega) = -i\omega\mathbf{a}_0(\omega) + \nabla\Phi$, i.e., the background quasi homogeneous acoustic flow plus the local flow generated by the micro-oscilator. By the ansatz Eq. (23), $\mathbf{x}$ is still defined in the rest system of the fluid, so the micro-oscillator–fluid coupling conditions of the eigenvalue problem are not affected.

The dynamic equation for the complete solution Eq. (23), i.e., an augmented version of Eq. (19), is

$$-\omega^2 \mathsf{M}\mathbf{a}^0 - \omega^2 \mathsf{T}\mathbf{x} + \mathsf{V}\mathbf{x} = \mathbf{F}, \qquad (24)$$

where $\mathbf{F}$ is the excitation force acting on the coupled system, i.e., the acoustic pressure force on the triangles distributed to their vertices by Eq. (9). We have considered that for a rigid motion $\mathbf{x}^{\text{tot}} = \mathbf{a}^0$ (thus $\mathbf{x} = 0$) there is no force other than $\mathbf{F}$ between the micro-oscilator and the fluid, and no force between the particles, $\mathsf{V}\mathbf{a}^0 = 0$. We thus have

$$-\omega^2 \mathsf{T}\mathbf{x} + \mathsf{V}\mathbf{x} = \mathbf{F} + \omega^2 \mathsf{M}\mathbf{a}^0, \qquad (25)$$

where $\omega^2 \mathsf{M}\mathbf{a}^0$ is interpreted as a system force — an additional excitation force acting on all particles, while $\mathbf{F}$ acts only on those on the surface. These forces generally excite relative motion between the interior of the micro-oscillator and its surface, resulting in hidden reaction forces on the fluid. As a check, in the case when the densities of the micro-oscillator and the fluid are equal, the sum of all force vectors in $\mathbf{F}$ (buoyancy) is equal and opposite to the total system force, and according to Eq. (25), $\mathbf{x} = 0$ is indeed a possible solution (which takes place when the excitation of the modes is negligible, e.g., for very low frequencies).

Writing $\mathbf{x} = \sum_i c_i |\mathbf{x}^i\rangle$ and using the bra–ket notation, the excited amplitudes c_i of the modes $|\mathbf{x}^i\rangle$ are obtained by projecting the dynamic equation Eq. (25) onto the modes. Taking into account the orthogonality Eq. (22), the mode amplitudes are

$$c_i = \frac{1}{\omega_i^2 - \omega^2} \frac{\langle \mathbf{x}^i | (\mathbf{F} + \omega^2 \mathsf{M}\mathbf{a}^0) \rangle}{\langle \mathbf{x}^i | \mathsf{T} | \mathbf{x}^i \rangle}, \qquad (26)$$

provided that all degenerate modes, Sec. II A, have been orthogonalized. We see that the effective mass matrix T, which also contains the mass load of the coupled fluid, appears in the denominator of Eq. (26) and reduces the mode amplitudes compared to the uncoupled case.

We regularize the singularities in Eq. (26) at $\omega^2 = \omega_i^2$ by introducing an imaginary part of ω_i, i.e., $\omega_i' \equiv \omega_i - i\beta_i$, while leaving the corresponding eigenmode unchanged. This is the classical Rayleigh damping, which is an adequate and standardly used approximation for the case of weak damping. Examples of sufficient conditions [54] for this type of damping are that the drag force supervector is proportional to $\mathsf{T}\mathbf{v}$ or $\mathsf{V}\mathbf{v}$, where $\mathbf{v}$ is the particle velocity supervector. Physically, this means that the damping force of a given mode is distributed to all micro-oscillator particles in proportion to their inertial or potential force amplitudes in that mode. We estimate the damping coefficients β_i, Eq. (A13) in a perturbative way by integrating from $r = r_0$ to $r = \infty$ the viscous dissipation for the unperturbed flow Eq. (11) coupled to the mode, Appendix A.

IV. HIDDEN FORCE AND SELF-CONSISTENT DYNAMIC DENSITY

To find the hidden force density $\mathbf{f}'$ of Eq. (1) which defines the effective dynamic density of the metafluid via Eqs. (2)-(3), we need to i) formulate the force of the micro-oscillator on the fluid arising from its excited modes Eq. (26) and ii) find a self-consistent excitation force $\mathbf{F}$ in Eq. (26) coming from the action of the continuous "sea" of other identical randomly oriented micro-oscillators in addition to the original acoustic pressure.

We regroup the terms of the dynamic equation Eq. (24) such that the form of Newton's law for individual particles with displacements Eq. (23) becomes transparent,

$$-\omega^2 \mathsf{M}(\mathbf{a}^0 + \mathbf{x}) = -\mathsf{V}\mathbf{x} + \omega^2 \mathsf{A}\mathbf{x} + \mathbf{F}. \qquad (27)$$

The interparticle forces $-\mathsf{V}\mathbf{x}$ are internal forces and drop out, $\mathbf{F}$ are due to the effective acoustic force acting everywhere in the fluid, while $\omega^2 \mathsf{A}\mathbf{x}$ are just the forces of interest — the additional forces of the fluid on the surface particles due to the coupled modes. Therefore, the total force of the excited micro-oscillator on the fluid is the negative sum of these force vectors,

$$\begin{aligned}
\mathbf{F}_1 &= -\omega^2 \sum_i \mathsf{A}\{\mathbf{x}_i\} \\
&= \omega^2 \sum_i \mathsf{M}\left(\{\mathbf{a}_0\} + \{\mathbf{x}_i\}\right) + \sum_i \{\mathbf{F}_i\} \\
&= \omega^2 m(\mathbf{a}_0 + \overline{\mathbf{x}}) - \omega^2 m_0 \mathbf{a}_0, \qquad (28)
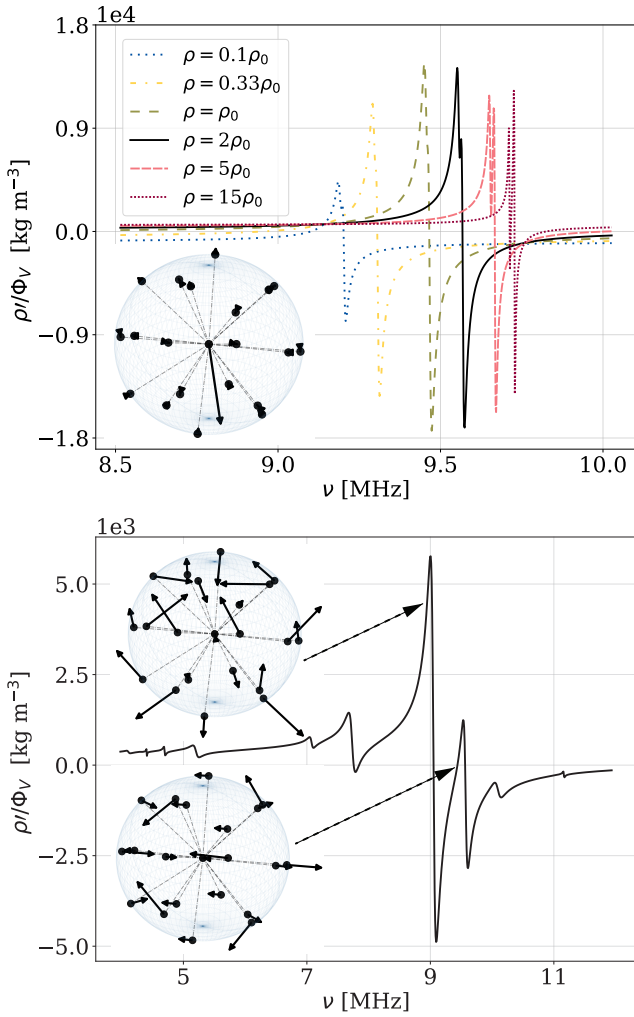\end{aligned}$$

Figure 2. Frequency dependence of dynamic density per volume concentration ρ'/ϕ_V for a simple micro-oscillator with one central and 20 surface points; all masses are equal. Top: the interactions between surface points are negligible, while those with the central point are equal. Bottom: the interactions with the central point are negligible, while all surface points interact equally with their nearest neighbours; $\rho = 2\rho_0$. Shown are some of the corresponding normal modes: in the upper case, the density effect results from the rigid relative motion of the shell with respect to the central mass, while in the lower case the effect is due solely to the motion of the surface points. Top (color/dashed): the dependence of the performance on the mass of the micro-oscillator with fixed size $r_0 = 3\,\mu\text{m}$. The splitting of the resonances, observed also in Fig. 3 (top), is due to a slight non-degeneracy of the depicted mode.

where m is the mass of the micro-oscillator, $\overline{\mathbf{x}}$ is the amplitude of the center of mass of the micro-oscillator modal motion, and m_0 is the mass of the fluid displaced by the micro-oscillator. The latter is just Archimedes' principle — the pressure force on a closed region of the fluid drives its acoustic motion $\mathbf{a}_0$; the equivalent continuous version of this statement is Eq. (1).

The hidden force density that follows from Eq. (28) is

$$\mathbf{f}' = \rho_N \mathbf{F}_1 = \omega^2 \rho_N \left[m\overline{\mathbf{x}} + (m - m_0)\mathbf{a}_0 \right]. \qquad (29)$$

Finally, one needs to find the excited $\overline{\mathbf{x}}$. We assume that $\overline{\mathbf{x}}$ lies along the axis defined by $\mathbf{a}_0$, which is true for an isotropic system, so in average it is also true for dispersion of orientationally disordered generally anisotropic micro-oscillators. The excited mode amplitudes Eq. (26) require $\mathbf{a}_0$ as well as $\mathbf{F}$, which requires knowledge of the pressure p, which in turn, to be connected to $\mathbf{a}_0$ by one of Eqs. (3) or (6), requires knowledge of the dynamic density or compressibility. In contrast, to compute $\overline{\mathbf{x}}$ in an isotropic linear system, only the gradient part of the local pressure is needed, but not its constant (homogeneous) part, since the excitation by homogeneous pressure cannot give a preferred direction and thus $\overline{\mathbf{x}} = 0$ by symmetry. (In a nonlinear system, the magnitude of $\overline{\mathbf{x}}$ would in general also depend on the homogeneous part of the pressure.)

¿From Eq. (1) it follows that the gradient of this local fluid pressure is nothing but $-\nabla p + \mathbf{f}'$ and is simply expressed by $-\omega^2 \rho_0 \mathbf{a}_0$. Thus, for the calculation of $\overline{\mathbf{x}}$, one obtains the excitation forces $\mathbf{F}_i$ on the surface particles, required in Eq. (26), from the local pressure field of the form

$$p_\nabla \equiv \omega^2 \rho_0 \mathbf{a}_0 \cdot \mathbf{r}, \qquad (30)$$

where $\mathbf{a}_0$ is constant, which agrees with Archimedes' principle considered in Eq. (28). With that, the force supervector in Eq. (26) is

$$\mathbf{F} = \{\mathbf{F}_i\} = -\omega^2 \rho_0 \tfrac{1}{3} \sum_{\triangle^k \ni i} \left\{ S^k \hat{\mathbf{n}}^k \left(\hat{\mathbf{e}}_0 \cdot \mathbf{R}^{\triangle^k} \right) \right\} a_0, \quad (31)$$

where the sum runs over triangles with vertex i and $\hat{\mathbf{e}}_0$ is a unit vector in the direction of $\mathbf{a}_0$.

An important result is that the self-consistent excitation of the mode amplitudes Eq. (26) and the self-consistent hidden force density Eq. (29) with $\overline{\mathbf{x}} = \sum_j \sum_i c_j(a_0) m_i \mathbf{x}_i^j$, where $\mathbf{x}_i^j$ is the displacement of particle i in mode j, are determined purely from the surface geometry and the modal structure of the micro-oscillator and are proportional to the amplitude $\mathbf{a}_0$ of the resulting acoustic wave.

Thus, if we write $\overline{\mathbf{x}} = (\overline{x}/a_0)\mathbf{a}_0$ with the awareness that $\overline{x}/a_0$ does not depend on $\mathbf{a}_0$ and is exclusively a property of the fluid-coupled micro-oscillator, with the hidden force density Eq. (29) we obtain a compact Euler equation Eq. (1) of the acoustic metafluid,

$$-\omega^2 \left[\rho_0 + \rho_N \left(m\frac{\overline{x}}{a_0} + (m - m_0) \right) \right] \mathbf{a}_0 = -\nabla p, \quad (32)$$

which in the square brackets explicitly defines an effective dynamic density

$$\rho^{\text{eff}}(\omega) = \rho_0 + \rho' = \rho_0 + \phi_V(\rho - \rho_0) + \phi_V \rho \frac{\overline{x}(\omega)}{a_0} \quad (33)$$

in terms of modal structure, mean mass density $\rho = m/V_1$ of the micro-oscillator with volume V_1, and their volume fraction $\phi_V = \rho_N V_1$ in the dilute limit. In Eq. (33), the first two terms reflect simple compositional average, while the last term represents the dynamic effect.

To build understanding step by step, we start with a minimal micro-oscillator model that produces the hidden force effect, Fig. 2 (top). It has both dipolar and breathing resonances; in our particular example they are around 9.5 MHz and 2.5 MHz in its basic design, but in general it is important that they are in the relevant ultrasonic range. A single central mass interacts with the shell, here represented by surface masses in an arrangement of the Thomson problem [55] and with negligible interactions between them. In other words, there is no in-surface elasticity, as is the case for a bubble. The central mass is needed in addition for the force effect, which is not present in the bubble. A single ρ' resonance is observed (black), corresponding to the relative motion of the central mass with respect to the surface. The situation changes significantly already if the in-surface elasticity is included, like in Fig. 2 (bottom), where the interaction with the central mass is negligible and thus this mass is irrelevant this time. Nevertheless, several ρ' resonances take place, corresponding to different modes of the surface particles alone.

This minimalistic example (and that of Fig. 4) is meant to illustrate the increasing complexity of the dynamic density response when the micro-oscillator becomes more complicated. Here and in all other cases, orientational averaging of the micro-oscillator was performed to describe an orientationally disordered metafluid and to cancel the artifacts (due to the discrete approximation of Eq. (12)) of a particular orientation with respect to the spherical basis. This ensures that $\overline{\mathbf{x}}$ and hence the hidden force are exactly parallel to the acoustic polarization $\mathbf{a}_0$ and a scalar effective density can indeed be defined as in Eqs. (3) and (32)-(33).

A. ρ' performance

To pursue the practically relevant question of which objects are better suited to generate a large negative dynamic density, heavier or lighter ones, Fig. 2 (top) also shows the dependence of ρ' on the mean density[2] ρ of the micro-oscillator with fixed size $r_0 = 3\,\mu\text{m}$, which is to be examined together with Eq. (33). The interparticle potential is rescaled proportionally to ρ so that the normal frequency of the *free* micro-oscillator remains unchanged. For the fluid-coupled micro-oscillator, the normal frequency therefore decreases slightly with decreas-

———

[2] Here we discuss only the effect of density scaling, while the more subtle effects of the distribution of mass and bond strength will be the focus of a follow-up study.
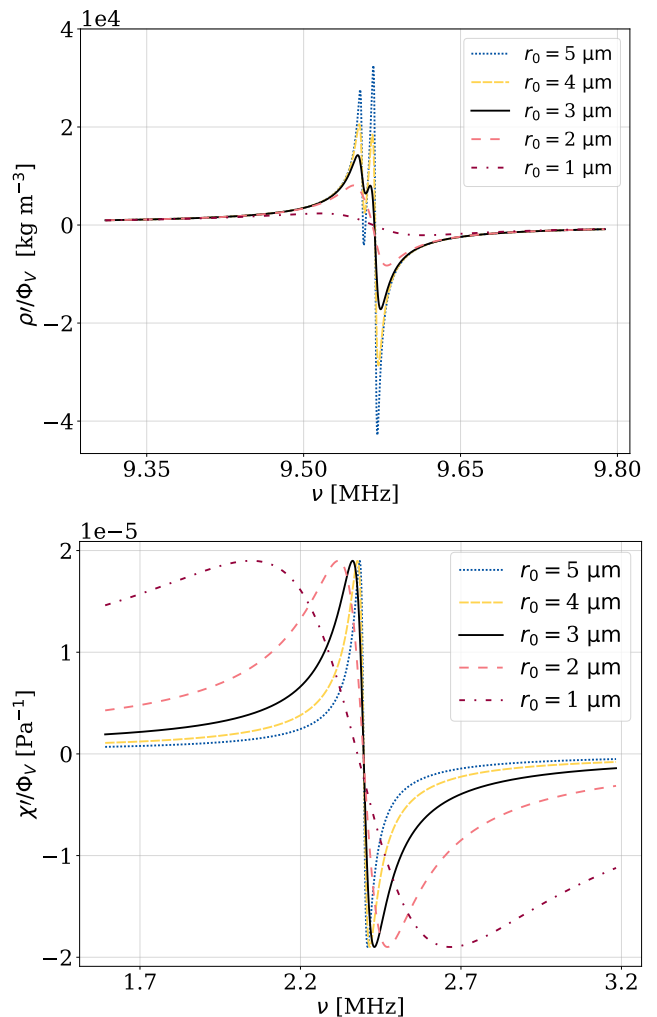

Figure 3. Dependence of ρ'/ϕ_V (top) and χ'/ϕ_V (bottom) on the size r_0 of the micro-oscillator, keeping its mean density fixed at $\rho = 2\rho_0$. The splitting of the resonances (top), already seen in Fig. 2 (top), is due to a slight non-degeneracy of the eigenmode in Fig. 2 (top).

ing ρ, as expected. The weak ρ' performance of low-density micro-oscillators is dictated by the ρ factor of Eq. (33), since the increasing $\overline{x}$ of lighter objects gets saturated by the finite fluid mass load. On the other hand, the performance of high-density micro-oscillators goes into saturation quite quickly. So we learn that the mean density of the micro-oscillator is not crucial as long as it is not much lower (e.g., in the case of hollow shells) than that of the host fluid.

Of practical interest is also the dependence of ρ'/ϕ_V on the size r_0 of the micro-oscillator, Fig. 3 (top), this time at fixed mean density ρ. Again, the potential between the particles was rescaled in proportion to their mass, leaving the uncoupled frequencies unchanged. But the effective fluid mass load also scales in the same proportion, so the frequencies of the fluid-coupled micro-oscillator also remain unchanged. What changes substantially is the

damping coefficient, which scales as $1/r_0^2$ according to Eq. (A13), as the coefficients Eq. (12) scale as r_0. Considering $\overline{x}$ of the simple mode of Fig. 2 (top) as an oscillator with eigenfrequency ω_0, damping coefficient β, *effective* mass m, driving force F and dynamic equation $(\omega_0^2 - \omega^2 - 2\mathrm{i}\omega\beta)\overline{x} = F/m$, the real part of its amplitude $\overline{x}(F)$ is $\mathrm{Re}(\overline{x}) = (F/m)(\omega^2 - \omega_0^2)/[(\omega^2 - \omega_0^2)^2 + (2\omega\beta)^2]$, which has the two extrema

$$\mathrm{Re}(\overline{x})_{1,2} \approx \pm \frac{F}{m}\frac{1}{4\beta\omega_0} \qquad (34)$$

at $\omega^2 - \omega_0^2 = \pm 2\beta\omega_0$. Since F/m is independent of r_0 in this case, the extrema of the dynamic part of ρ' are thus inversely proportional to the damping coefficient, so that the performance falls sharply as the size of the micro-oscillator decreases. This is indeed confirmed by Fig. 3 (top).

Recall that the estimate of the damping coefficient Eq. (A13) is based on potential flow and is therefore an overestimate for situations with strong damping. Nevertheless, the general message is that damping is a critical limiting factor for metafluid systems. As Fig. 3 (top) suggests, this problem can be overcome with sufficiently large micro-oscillators — a reasonable estimate of the critical scale is 1 μm.

V. HIDDEN VOLUME SOURCE AND SELF-CONSISTENT DYNAMIC COMPRESSIBILITY

To find the hidden volume source density q' of Eq. (4) which defines the effective dynamic compressibility of the metafluid via Eqs. (5)-(6), we need to formulate the volume source of the micro-oscillator arising from its excited modes Eq. (26). This time the excitation with the actual, full pressure of the fluid is relevant.

One sees that in the long-wavelength limit the local pressure p' exerting on the fluid the hidden force $\mathbf{f}'$ in Eq. (1) is negligible with respect to p, although in the metaregime $\mathbf{f}'$ is comparable to ∇p. This looks paradoxical at first glance, but it is not: p builds up from ∇p on the length scale of the wavelength, whereas p' builds up from $-\mathbf{f}'$ on the length scale of the inter-micro-oscillator spacing — the micro-oscilator pushes the fluid at the front with increased pressure and pulls it at the back with decreased pressure. From the point of view of the continuum: to accelerate an extended region of the fluid, a large pressure such as p must be applied to its boundary, while no such pressure is required if the accelerating force, like $\mathbf{f}'$, is distributed in the volume.

Thus, $\mathbf{F}$ in Eq. (26) is given by the pressure p. The second term in this equation can also be expressed by p via Eq. (3),

$$\omega^2 \mathsf{M}\mathbf{a}^0 = \omega^2\{m_i\}\mathbf{a}_0 = \{m_i\}\frac{\mathrm{i}\mathbf{k}}{\rho^{\mathrm{eff}}}p, \qquad (35)$$

which is out of phase with the first term. This would make dynamic compressibility inherently complex and would be a problem for the metaregime. However, one sees two things. i) In a free micro-oscillator, this term excites only rigid translation modes with no volume change and is orthogonal to all other modes. Only the coupling with the fluid makes this term in general not perfectly orthogonal to other modes. ii) Comparing the force on a surface particle from the second and first terms of Eq. (26), the ratio of their magnitudes can be estimated to $\sim (\rho/\rho^{\mathrm{eff}})kd$, where d is an effective thickness of the surface layer. Unless ρ^{eff} is close to zero, the ratio of the magnitudes in the long-wavelength limit is tiny.

Therefore, we neglect the second term of Eq. (26), while the force supervector of its first term is

$$\mathbf{F} = \{\mathbf{F}_i\} = -\tfrac{1}{3}\sum_{\triangle^k \ni i}\left\{S^k\hat{\mathbf{n}}^k\right\}p, \qquad (36)$$

where the sum runs over triangles with vertex i. The volume flux of the micro-oscillator is

$$Q_1 = -\mathrm{i}\omega\sum_{\triangle^k}\tfrac{1}{3}\sum_{i\in\triangle^k}S^k\hat{\mathbf{n}}^k\cdot\mathbf{x}_i \equiv S_1\tilde{Q}_1, \qquad (37)$$

where the first sum is over all triangles, the second over the vertices of a triangle and $\mathbf{x}_i = \sum_j c_j(p)\mathbf{x}_i^j$ are proportional to p. For a given dynamics, Q_1 scales with the surface area of the micro-oscillator, while its surface density $\tilde{Q}_1 = Q_1/S_1$, where S_1 is the total surface area of the micro-oscillator, remains unaffected.

Knowing that $Q_1/(\mathrm{i}\omega p)$ does not depend on p and is exclusively a property of the fluid-coupled micro-oscillator, we write $Q_1 = \mathrm{i}\omega p\, Q_1/(\mathrm{i}\omega p)$. With the hidden volume source density $q' = \rho_N\, \mathrm{i}\omega p\, Q_1/(\mathrm{i}\omega p)$ we obtain a compact continuity/compressibility equation Eq. (4) of the acoustic metafluid,

$$-\mathrm{i}\omega\left(\chi_0 + \rho_N\frac{Q_1}{\mathrm{i}\omega p}\right)p + \nabla\cdot\mathbf{u} = 0, \qquad (38)$$

which explicitly defines an effective dynamic compressibility

$$\chi^{\mathrm{eff}} = \chi_0 + \chi' = \chi_0 + \phi_V\frac{S_1}{V_1}\frac{\tilde{Q}_1}{\mathrm{i}\omega p} \qquad (39)$$

in terms of modal structure and volume fraction ϕ_V of the micro-oscillators in the dilute limit. The surface to volume ratio S_1/V_1 reflects the fact that for a given volume flux density $\tilde{Q}_1$ from the surface of the micro-oscillator (the mean velocity of the surface) its relative volume change rate is inversely proportional to its linear size. Alternatively, one can simply write in Eq. (39) $\phi_V S_1/V_1 \equiv \phi_S$, where ϕ_S is the total surface area of the micro-oscillators per volume of the metafluid, intuitively suggesting that the "active region" is indeed the surface of the micro-oscillators.

Fig. 4 (top) shows the dynamic compressibility spectrum of our simple model micro-oscillator from Sec. IV, whose breathing mimics that of a bubble: there is no
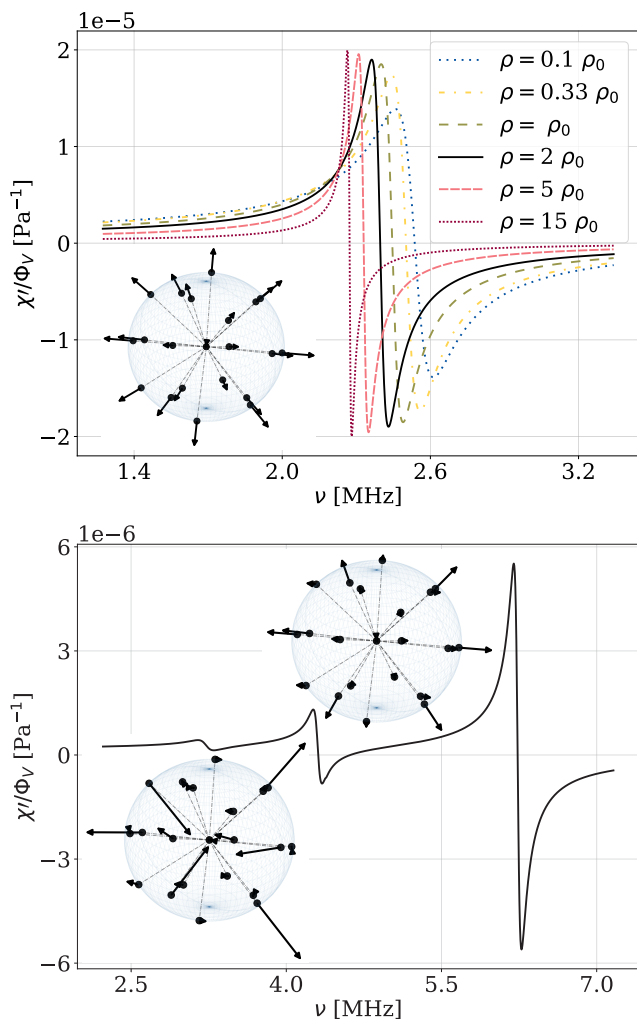
Figure 4. Frequency dependence of dynamic compressibility per volume concentration χ'/ϕ_V for the simple micro-oscillator model of Fig. 2. Top: the interactions between surface points are negligible. Bottom: the interactions with the central point are negligible; $\rho = 2\rho_0$. Shown are some of the corresponding normal modes. Top (color/dashed): the dependence of the performance on the mass of the micro-oscillator with fixed size $r_0 = 3\,\mu\mathrm{m}$.

surface elasticity and the compressional function of the trapped gas is taken over by the isotropic interaction with the central point, which is otherwise obsolete. A single breathing mode results (black), and because of mode orthogonality, this is the only volume-changing mode that exists for a bubble. But even simple surface elasticity relaxes this constraint, and many different resonances begin to contribute to the volume change, Fig. 4 (bottom).

A. χ' performance

We are again interested in the practical question of which objects produce a larger negative compressibility, heavier

or lighter ones. Fig. 4 (top) shows the dependence of χ' on the mean density ρ of the micro-oscillator with fixed size $r_0 = 3\,\mu\mathrm{m}$. In this case, the interparticle potential was rescaled taking into account the fluid mass load Eq. (21), such that the normal frequency of a perfect fluid-coupled breathing sphere would remain unchanged. It is well seen that the damping coefficient decreases with increasing ρ, which is in agreement with the factor $\langle \mathbf{x}^i | \mathbf{T} | \mathbf{x}^i \rangle$ in the denominator of Eq. (A13). Yet the peak height of χ' shows only a weak dependence on ρ. Why is this so? Similar to our earlier consideration leading to Eq. (34), this time we consider $\tilde{Q}_1/(i\omega) = -x$ of the simple breathing mode, Fig. 4 (top), as an oscillator with x the radial amplitude of the surface particles. Thus, the extrema of $\tilde{Q}_1/(i\omega)$ are again given by Eq. (34). However, this time F is constant there, while the product $m\beta$ in the denominator is also constant according to Eq. (A13), as for a given modal shape it depends only on r_0. Therefore, the weak density dependence observed in Fig. 2 (top) is actually due to the factor $1/\omega_0$ of Eq. (34). We can conclude that the bandwidth of the χ' performance decreases with increasing the mean density of the micro-oscillator, while the peak amplitude is independent of it.

Fig. 3 (bottom) shows the dependence of χ'/ϕ_V on the size r_0 of the micro-oscillator with fixed mean density ρ. As in Fig. 3 (top), the potential between the particles has been rescaled in proportion to their mass, leaving both uncoupled and coupled normal frequencies unchanged. Again, the damping coefficient scales as $1/r_0^2$. However, unlike ρ'/ϕ_V in Fig. 3 (top), in our simple oscillator model the driving force F of Eq. (34) is now proportional to the surface area of the micro-oscillator rather than its volume, so that $\tilde{Q}_1/(i\omega)$ gets a factor of $F/m = 1/r_0$. Together with the factor $1/r_0$ in Eq. (39) this compensates for the inverse proportionality of χ'/ϕ_V peaks to the damping, Eq. (34), making their heights exactly independent of r_0. Physically speaking, the lower damping of a larger micro-oscillator is cancelled out by a weaker driving force relative to its larger mass. In effect, the bandwidth of the χ' performance decreases sharply with the size of the micro-oscillator, while the peak amplitude is again independent.

VI.   TOWARDS A REALISTIC SCENARIO

To go beyond the pure examples shown earlier and get a sense of a more realistic situation, Fig. 5 (bottom) shows as an example the dynamic density performance of a more complicated and less regular micro-oscillator consisting of 30 surface and 50 internal particles with random positions and varying potentials, Fig. 5 (top). The idea behind this still rather simple example is to model a heterogeneous macromolecule, in which different structural units with higher stiffness interact in a less stiff manner, as is typical for proteins. In particular, due to the possibility of low-frequency floppy modes in such discrete heterogeneous structures [41–45], their dynamic proper-
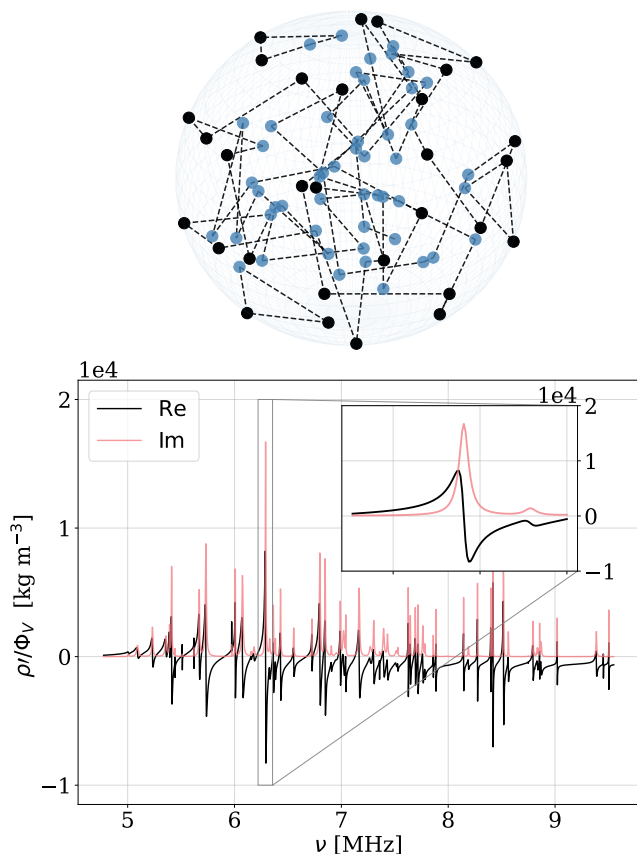
Figure 5. Top: a heterogeneous micro-oscillator model consisting of 30 surface (black) and 50 internal (color) particles with random positions and varying potentials; dashed lines indicate strong bonds. Bottom: the corresponding dynamic density spectrum — real (black) and imaginary (color) parts of the complex quantity ρ'/ϕ_V, Eq. (33). Inset: close-up of the frequency response of the two parts near a resonance.

ties can differ significantly from those of uniform elastic objects, and it is precisely such effects that one would like to exploit in the development of a metafluid. We will investigate these issues in future studies using extensive micro-oscillator models of the type shown in Fig. 5 (top).

Fig. 5 (bottom) reminds us that in general there may be many frequency windows of potential interest. This time we also show the imaginary part of the dynamic modulus, which was omitted in all previous figures. It represents energy loss and cannot be negative. The inset shows the detailed behavior of the complex quantity ρ'/ϕ_V near a resonance and unveils the standard resonant response of the real and imaginary parts of the compliance. Exactly at the resonance, where the real part is zero and the imaginary part is maximum, there is only damping, i.e., strong scattering and no wave propagation. The frequency windows of a transparent metafluid lie to the right of the resonances where the imaginary part of ρ' is already small while the real part is still large and negative. Provided, of course, that in the same frequency

window the same is true for χ'.

In this work we have treated the suspension in the dilute limit, where direct interactions between the oscillators are neglected. For larger micro-oscillator densities, one can resort to methods of mesoscopic simulations. In a preliminary study, we have set-up a coupled molecular dynamics (micro-oscillator)–Lattice-Boltzmann [56] (solvent) simulation, where the interaction between the micro-oscillator beads and the solvent is implemented by the immersed boundary method [57, 58]. In qualitative agreement with the harmonic analysis presented in this work, we show that the pressure waves induce a motion of the center of mass of the micro-oscillator, Fig. 6. At the right frequency, the micro-oscillator moves in the opposite direction as the fluid, Fig. 6 (bottom), decreasing the effective density of the system.

VII. SUMMARY AND CONCLUSION

Let us recapitulate the distinguishing features of the presented metafluid model. i) It is a model of a fluid metamaterial without the support of an external skeletal structure providing external reaction forces. Instead, these come from the inner, hidden part of the micro-oscillator, which must be effectively inaccesible to the host fluid. ii) The operation of such metafluids is not based on spatial organization of the micro-oscillators. iii) The modal shapes of the micro-oscillators are generally irregular, as is normally true also for biological or macromolecular objects. In principle, this generalization does not pose a problem for the meta-behavior and opens more frequency windows as candidates for a suitable meta-regime. Moreover, the discrete, irregular, heterogeneous micro-oscillator structure with different local connections (e.g. interconnected filaments, sheets, clumps) is thought to allow for dynamic surprises not expected from quasi-homogeneous elastic systems, such as floppy modes, which extend the low-frequency range and could also lead to anomalous, stronger hidden force effects.

We should not overlook one characteristic feature. The results show that the dynamic compressibility effect χ'/χ_0 is much larger than the dynamic density effect ρ'/ρ_0, cf. Figs. 2 and 4. In our minimal models, this is directly due to design, i.e., the choice of an appropriately weak interparticle potential to keep the normal frequencies low enough. But in reality it is similar — compared to the displaced volume of the host fluid, complex molecules have much lower breathing frequencies due to voids and numerous ways to move orthogonally to strong bonds. This means that such a (bio)macromolecular metafluid will tend to have large negative effective compressibility and smaller negative effective density relative to the moduli of the host fluid. This apparently convenient circumstance allows the speed of the meta-ultrasound $c = (\chi^{\mathrm{eff}} \rho^{\mathrm{eff}})^{-1/2}$ to be kept close to the original ultrasound speed in the host fluid. For the same rea-
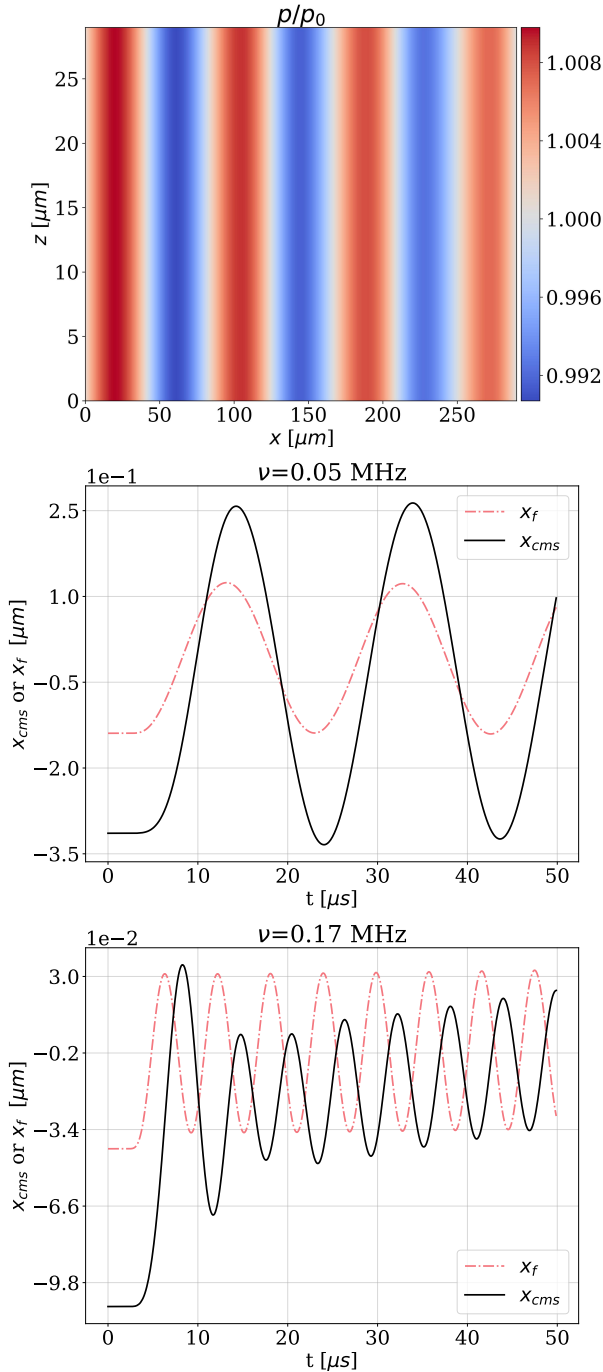
Figure 6. Top: normalized pressure field p/p_0 profile in the xz plane of an acoustic wave traveling to the right at $\nu = 0.05$ MHz. A micro-oscillator of the type of Fig. 2 (but with different masses, spring constant, and size) is located at $x = y = z = 14.5\,\mu$m. Mean-subtracted center of mass of the micro-oscillator x_{cms} and the average displacement of the fluid x_f (evaluated at the initial center of mass of the micro-oscillator) at $\nu = 0.05$ MHz (middle) and $\nu = 0.17$ MHz (bottom). In the latter case, the micro-oscillator and the fluid move almost out of phase.

son, however, the specific impedance $z = (\rho^{\mathrm{eff}}/\chi^{\mathrm{eff}})^{1/2}$ of a metafluid will be low — this seems to be a characteristic property of metafluids of this type!

Not surprisingly, our results show that damping is a crucial limiting factor for the metafluid systems described. More precisely, as best seen in Fig. 3, it is only crucial for the dynamic density mechanism, but not for the compressibility. The reasons for this rather interesting distinction were discussed in Sec. V A. This confirms that a sufficient hidden force effect is the main challenge in metafluids.

The specific intrinsic damping within the micro-oscillator was not considered in our model. It should be small or at most comparable to the viscous damping in the solvent. Reasonable candidates for micro-oscillators are therefore macromolecules. The damping of isolated molecules is negligible compared to the damping caused by contact with the solvent. Also suitable would be artificial, e.g., microprinted oscillators. Not to be excluded a priori are lyotropic lipid bilayer structures such as multilamellar vesicles if they are in the solid (gel) state, while microbiological objects are generally overdamped.

Nevertheless, damping at the microscopic scale was taken into account by integrating the dissipation down to the size of the microoscillator r_0. This also effectively captures the specific dissipation at the contact between the solvent and the microoscillator by slightly redefining r_0. Here, the dissipation is primarily due to the local reconfiguration of the trapped solvent molecules in response to the changing configuration of the micro-oscillator and should be sufficiently small. This requirement is compatible with the assumption in Sec. II that the interior of the micro-oscillator should be inaccessible to the solvent, which is necessary in the case of potential flow. In general, it is essential for the compressibility effect, but perhaps not necessarily for the density effect, which in principle could also be based on viscous coupling with the fluid.

VIII. ACKNOWLEDGMENTS

Appendix A: Viscous dissipation and mode damping

The damping of the coupled modes Eq. (22) is estimated by calculating viscous dissipation (time-averaged heat production rate) P in the volume of the surrounding fluid for the unperturbed potential flow Eq. (11) of the fluid,

$$P = \frac{1}{2} \int \mathrm{d}V\, \sigma_{ij}^{v*} v_{ij} = \eta \int \mathrm{d}V\, v_{ij}^* v_{ij}, \qquad \text{(A1)}$$

where $\sigma_{ij} = 2\eta v_{ij}$ is the viscous stress tensor, η is the viscosity, and $v_{ij} = \frac{1}{2}(\partial_i v_j + \partial_j v_i)$ is the strain rate tensor. Such a perturbation treatment is a good approximation for the weak damping case.

The velocity field Eq. (11) is

$$\mathbf{v}(\mathbf{r}) = \nabla \Phi = \sum_{l,m} b_{lm}(R'_l Y_{lm}\hat{\mathbf{r}} + R_l \nabla Y_{lm}), \qquad \text{(A2)}$$

where $R_l(r) = (r/r_0)^{-(l+1)}$, $\hat{\mathbf{r}} = \mathbf{r}/r$, and ∇ is the angular part of ∇, while the strain rate tensor is

$$v_{ij} = \sum_{l,m} b_{lm} \bigg(R''_l Y_{lm}\hat{\mathbf{r}} \otimes \hat{\mathbf{r}} + 2R'_l[\nabla Y_{lm} \otimes \hat{\mathbf{r}}]^S$$
$$+ \frac{R'_l}{r} Y_{lm}(\mathsf{I} - \hat{\mathbf{r}} \otimes \hat{\mathbf{r}}) + R_l \nabla \otimes \nabla Y_{lm} \bigg), \qquad \text{(A3)}$$

where $[\quad]^S$ denotes symmetrization. We use here the usual complex spherical harmonics Y_{lm} and the coefficients b_{lm} are now proper complex combinations of b_{lm} and $b_{l,-m}$ of Eq. (11). However, since the final result is independend of this transformation, we keep the notation b_{lm} unchanged.

It can be shown that any tensor field (like v_{ij}) can be expanded in terms of an orthogonal set of *tensor spherical harmonics* [59, 60]. Following ref. [61], see the equations (2.28b), (2.30a)-(2.30d) therein, we write down the dyadic terms of Eq. (A3):

$$Y_{lm}\hat{\mathbf{r}} \otimes \hat{\mathbf{r}} = \left(\frac{(l+1)(l+2)}{(2l+1)(2l+3)} \right)^{1/2} \mathsf{T}^{2,l+2,lm}$$
$$- \left(\frac{2l(l+1)}{3(2l-1)(2l+3)} \right)^{1/2} \mathsf{T}^{2,l,lm}$$
$$+ \left(\frac{l(l-1)}{(2l-1)(2l+1)} \right)^{1/2} \mathsf{T}^{2,l-2,lm}$$
$$- \frac{1}{\sqrt{3}} \mathsf{T}^{0,l,lm}, \qquad \text{(A4)}$$

$$r[\nabla Y_{lm} \otimes \hat{\mathbf{r}}]^S = - \left(\frac{l^2(l+1)(l+2)}{(2l+1)(2l+3)} \right)^{1/2} \mathsf{T}^{2,l+2,lm}$$
$$- \left(\frac{3l(l+1)}{2(2l-1)(2l+3)} \right)^{1/2} \mathsf{T}^{2,l,lm}$$
$$+ \left(\frac{l(l-1)(l+1)^2}{(2l-1)(2l+1)} \right)^{1/2} \mathsf{T}^{2,l-2,lm}, \qquad \text{(A5)}$$

$$Y_{lm}(\mathsf{I} - \hat{\mathbf{r}} \otimes \hat{\mathbf{r}}) = - \left(\frac{(l+1)(l+2)}{(2l+1)(2l+3)} \right)^{1/2} \mathsf{T}^{2,l+2,lm}$$
$$+ \left(\frac{2l(l+1)}{3(2l-1)(2l+3)} \right)^{1/2} \mathsf{T}^{2,l,lm}$$
$$- \left(\frac{l(l-1)}{(2l-1)(2l+1)} \right)^{1/2} \mathsf{T}^{2,l-2,lm}$$
$$- \frac{2}{\sqrt{3}} \mathsf{T}^{0,l,lm}, \qquad \text{(A6)}$$

$$r^2 \nabla \otimes \nabla Y_{lm} = \left(\frac{l^2(l-1)^2(l+1)(l+2)}{4(2l+1)(2l+3)} \right)^{1/2} \mathsf{T}^{2,l+2,lm}$$
$$+ \left(\frac{3l(l+1)(l-1)^2(l+2)^2}{2(2l-1)(2l+3)} \right)^{1/2} \mathsf{T}^{2,l,lm}$$
$$+ \left(\frac{(l+2)^2(l+1)^2l(l-1)}{4(2l-1)(2l+1)} \right)^{1/2} \mathsf{T}^{2,l-2,lm}$$
$$+ \frac{1}{\sqrt{3}}l(l+1)\mathsf{T}^{0,l,lm}, \qquad \text{(A7)}$$

where $\mathsf{T}^{2,l',lm}$ represent, for a given l and m, five symmetric basis tensors ($l' = l \pm (0, 1, \text{ or } 2)$) while $\mathsf{T}^{0,l,lm} = -\frac{1}{\sqrt{3}}Y^{lm}\mathsf{I}$. The expression Eq. (A7) is given explicitly in equation (6a) of ref. [60].

The $\mathsf{T}^{\lambda,l,LM}$ basis tensor spherical harmonics are orthonormal [61] under the scalar product

$$\int d\Omega \, T_{jk}^{\lambda',l',L'M'*} T_{jk}^{\lambda,l,LM} = \delta_{\lambda\lambda'}\delta_{ll'}\delta_{LL'}\delta_{MM'}, \qquad \text{(A8)}$$

where the integral is performed over the solid angle Ω. The calculation of the dissipated power Eq. (A1) is therefore rather straightforward and after integrating from $r = r_0$ to $r = \infty$ gives

$$P = \frac{\eta}{r_0} \sum_{l,m} |b_{lm}|^2 (l+1)(l+2)(2l+1). \qquad \text{(A9)}$$

Assuming for an eigenfrequency, Eq. (22),

$$\omega_i' \equiv \omega_i - \mathrm{i}\beta_i, \qquad (A10)$$

the mode amplitude decays as $\mathrm{e}^{-\beta_i t}$ and its total energy W as $\mathrm{e}^{-2\beta_i t}$, thus

$$\dot{W} = -2\beta_i W. \qquad (A11)$$

Using in Eq. (A11) for $-\dot{W}$ the result Eq. (A9) and the amplitude of the total kinetic energy of the coupled mode (including the kinetic energy of the coupled fluid)

$$W = \frac{1}{2}\omega_i^2 \langle \mathbf{x}^i | \mathsf{T} | \mathbf{x}^i \rangle \qquad (A12)$$

for its total energy, one gets the mode damping coefficient

$$\begin{aligned}\beta_i &= \frac{P(\omega_i, \mathbf{x}^i)}{\omega_i^2 \langle \mathbf{x}^i | \mathsf{T} | \mathbf{x}^i \rangle} \qquad (A13)\\ &= \frac{\eta}{r_0}\frac{1}{\omega_i^2 \langle \mathbf{x}^i | \mathsf{T} | \mathbf{x}^i \rangle}\sum_{l,m}|b_{lm}^i|^2(l+1)(l+2)(2l+1),\end{aligned}$$

where $b_{lm}^i \propto \omega_i$ correspond to the mode $|\mathbf{x}^i\rangle$.

There is one detail to add. Due to the restriction to irrotational flow Eq. (11), those normal modes, which on the surface of the micro-oscillator happen to be mainly tangential, are only weakly coupled to the fluid. Notwithstanding the fact that these modes are less excited by the pressure and their contribution to the micro-oscillator volume source Q_1 and force F_1 is relatively insignificant, it could be dangerous if their damping were unphysically small. To eliminate this problem, we scale the dissipation $P(\omega_i, \mathbf{x}^i)$ of a mode — knowing that it comes only from the radial components of the surface particles — by the ratio of the sum of squares of radial components and the sum of squares of full displacements of the surface particles.

[1] M. Kadic, T. Bückmann, R. Schittny, and M. Wegener, Reports on Progress in Physics **76**, 126501 (2013), URL https://doi.org/10.1088%2F0034-4885%2F76%2F12%2F126501.

[2] S. A. Cummer, J. Christensen, and A. Alù, Nature Reviews Materials **1**, 16001 (2016), ISSN 2058-8437.

[3] M. Kadic, G. W. Milton, M. van Hecke, and M. Wegener, Nature Reviews Physics **1**, 198 (2019), URL https://www.nature.com/articles/s42254-018-0018-y.

[4] S. H. Lee, C. M. Park, Y. M. Seo, Z. G. Wang, and C. K. Kim, Phys. Rev. Lett. **104**, 054301 (2010), URL https://link.aps.org/doi/10.1103/PhysRevLett.104.054301.

[5] V. M. García-Chocano, R. Graciá-Salgado, D. Torrent, F. Cervera, and J. Sánchez-Dehesa, Phys. Rev. B **85**, 184102 (2012), URL https://link.aps.org/doi/10.1103/PhysRevB.85.184102.

[6] J. J. Park, C. M. Park, K. J. B. Lee, and S. H. Lee, Applied Physics Letters **106**, 051901 (2015), https://doi.org/10.1063/1.4907634, URL https://doi.org/10.1063/1.4907634.

[7] S. Zhang, L. Yin, and N. Fang, Physical review letters **102**, 194301 (2009).

[8] S. Zhai, H. Chen, C. Ding, and X. Zhao, Journal of Physics D Applied Physics **46**, 5105 (2013).

[9] Y. Wang, C. Luo, Y. Dong, S. Zhai, C. Ding, and X. Zhao, Journal of Physics D: Applied Physics **52**, 085601 (2018).

[10] M. Boccaccio, P. Rachiglia, G. P. Malfense Fierro, G. Pio Pucillo, and M. Meo, Sensors **21** (2021), ISSN 1424-8220, URL https://www.mdpi.com/1424-8220/21/4/1170.

[11] J. Wang, F. Allein, N. Boechler, J. Friend, and O. Vazquez-Mena, Phys. Rev. Applied **15**, 024025 (2021), URL https://link.aps.org/doi/10.1103/PhysRevApplied.15.024025.

[12] J. Christensen and F. J. G. de Abajo, Phys. Rev. Lett. **108**, 124301 (2012), URL https://link.aps.org/doi/10.1103/PhysRevLett.108.124301.

[13] Z. Liang and J. Li, Phys. Rev. Lett. **108**, 114301 (2012), URL https://link.aps.org/doi/10.1103/PhysRevLett.108.114301.

[14] T. Frenzel, J. David Brehm, T. Bückmann, R. Schittny, M. Kadic, and M. Wegener, Applied Physics Letters **103**, 061907 (2013), https://doi.org/10.1063/1.4817934, URL https://doi.org/10.1063/1.4817934.

[15] A. Baz, New Journal of Physics **11**, 123010 (2009).

[16] B.-I. Popa and S. Cummer, Physical Review B **88** (2013).

[17] L. Sirota, D. Sabsovich, Y. Lahini, R. Ilan, and Y. Shokef, Mechanical Systems and Signal Processing **153**, 107479 (2021).

[18] T. Neil, Z. Shen, D. Robert, B. Drinkwater, and M. Holderied, Proceedings of the National Academy of Sciences of the United States of America **117**, 31134 (2020), ISSN 0027-8424.

[19] H. Ammari, B. Fitzpatrick, D. Gontier, H. Lee, and H. Zhang, Annales de l'Institut Henri Poincaré C, Analyse non linéaire **35**, 1975 (2018), ISSN 0294-1449, URL http://www.sciencedirect.com/science/article/pii/S0294144918300362.

[20] V. Leroy, N. Chastrette, M. Thieury, O. Lombard, and A. Tourin, Fluids **3**, 95 (2018), URL https://doi.org/10.3390/fluids3040095.

[21] M. Lanoy, J. H. Page, G. Lerosey, F. Lemoult, A. Tourin, and V. Leroy, Phys. Rev. B **96**, 220201 (2017), URL https://link.aps.org/doi/10.1103/PhysRevB.96.220201.

[22] V. Leroy, A. Strybulevych, M. Lanoy, F. Lemoult, A. Tourin, and J. H. Page, Phys. Rev. B **91**, 020301 (2015), URL https://link.aps.org/doi/10.

1103/PhysRevB.91.020301.

[23] M. Lanoy, R. Pierrat, F. Lemoult, M. Fink, V. Leroy, and A. Tourin, Phys. Rev. B **91**, 224202 (2015), URL https://link.aps.org/doi/10.1103/PhysRevB.91.224202.

[24] V. Leroy, A. Strybulevych, M. G. Scanlon, and J. H. Page, The European Physical Journal E **29**, 123 (2009), URL https://doi.org/10.1140/epje/i2009-10457-y.

[25] P.-G. Luan, Crystals **9**, 457 (2019), URL https://doi.org/10.3390/cryst9090457.

[26] J. Li and C. T. Chan, Phys. Rev. E **70**, 055602 (2004), URL https://link.aps.org/doi/10.1103/PhysRevE.70.055602.

[27] L. Saviot, C. H. Netting, and D. B. Murray, The Journal of Physical Chemistry B **111**, 7457 (2007), pMID: 17547453, https://doi.org/10.1021/jp071765x, URL https://doi.org/10.1021/jp071765x.

[28] V. Galstyan, O. S. Pak, and H. A. Stone, Physics of Fluids **27**, 032001 (2015), https://doi.org/10.1063/1.4914045, URL https://doi.org/10.1063/1.4914045.

[29] Z. Boltaev, I. Safarov, and T. Razokov, International Journal of Scientific & Technology Research **9**, 3674 (2020).

[30] J. Mei, Z. Liu, W. Wen, and P. Sheng, Phys. Rev. Lett. **96**, 024301 (2006), URL https://link.aps.org/doi/10.1103/PhysRevLett.96.024301.

[31] Y. Ding, Z. Liu, C. Qiu, and J. Shi, Phys. Rev. Lett. **99**, 093904 (2007), URL https://link.aps.org/doi/10.1103/PhysRevLett.99.093904.

[32] Z. Liu, C. T. Chan, and P. Sheng, Phys. Rev. B **71**, 014103 (2005), URL https://link.aps.org/doi/10.1103/PhysRevB.71.014103.

[33] E. Kurihara, T. A. Hay, Y. A. Ilinskii, E. A. Zabolotskaya, and M. F. Hamilton, The Journal of the Acoustical Society of America **130**, 3357 (2011), https://doi.org/10.1121/1.3626137, URL https://doi.org/10.1121/1.3626137.

[34] T. Brunet, A. Merlin, B. Mascaro, K. Zimny, J. Leng, O. Poncelet, C. Aristégui, and O. Mondain-Monval, Nature Materials **14**, 384 (2015).

[35] J. R. Lindner, Nat. Rev. Drug Discov. **3**, 527 (2004).

[36] N. Deshpande, A. Needles, and J. K. Willmann, Clin. Radiol. **65**, 567 (2010).

[37] H. Lee, H. Kim, H. Han, M. Lee, S. Lee, H. Yoo, J. H. Chang, and H. Kim, Biomed. Eng. Lett. **7**, 59 (2017).

[38] D. Maresca, A. Lakshmanan, M. Abedi, A. Bar-Zion, A. Farhadi, G. J. Lu, J. O. Szablowski, D. Wu, S. Yoo, and M. G. Shapiro, Annu. Rev. Chem. Biomol. Eng. **9**, 229 (2018).

[39] T. Brunet, S. Raffy, B. Mascaro, J. Leng, R. Wunenburger, O. Mondain-Monval, O. Poncelet, and C. Aristégui, Applied Physics Letters **101**, 011913 (2012).

[40] N. Kaina, F. Lemoult, M. Fink, and G. Lerosey, Nature **525**, 77 (2015), URL https://doi.org/10.1038/nature14678.

[41] A. J. Rader, B. M. Hespenheide, L. A. Kuhn, and M. F. Thorpe, Proceedings of the National Academy of Sciences **99**, 3540 (2002), https://www.pnas.org/doi/pdf/10.1073/pnas.062492699, URL https://www.pnas.org/doi/abs/10.1073/pnas.062492699.

[42] M. V. Chubynsky and M. F. Thorpe, Phys. Rev. E **76**, 041135 (2007), URL https://link.aps.org/doi/10.1103/PhysRevE.76.041135.

[43] L. Meireles, M. Gur, A. Bakan, and I. Bahar, Protein Science **20**, 1645 (2011), https://onlinelibrary.wiley.com/doi/pdf/10.1002/pro.711, URL https://onlinelibrary.wiley.com/doi/abs/10.1002/pro.711.

[44] S. Mahajan and Y.-H. Sanejouand, Archives of Biochemistry and Biophysics **567**, 59 (2015), ISSN 0003-9861, URL https://www.sciencedirect.com/science/article/pii/S0003986114004457.

[45] M. Habibi, S. S. Plotkin, and J. Rottler, Biophysical Journal **114**, 562 (2018), ISSN 0006-3495, URL https://www.sciencedirect.com/science/article/pii/S0006349517350439.

[46] A. R. Atilgan, S. R. Durell, R. L. Jernigan, M. C. Demirel, O. Keskin, and I. Bahar, Biophysical Journal **80**, 505 (2001).

[47] E. Eyal, L.-W. Yang, and I. Bahar, Bioinformatics **22**, 2619 (2006), ISSN 1367-4803, https://academic.oup.com/bioinformatics/article-pdf/22/21/2619/697193/btl448.pdf, URL https://doi.org/10.1093/bioinformatics/btl448.

[48] E. Eyal, A. Dutta, and I. Bahar, WIREs Computational Molecular Science **1**, 426 (2011), https://wires.onlinelibrary.wiley.com/doi/pdf/10.1002/wcms.44, URL https://wires.onlinelibrary.wiley.com/doi/abs/10.1002/wcms.44.

[49] J. M. M. Pinkerton, Proceedings of the Physical Society. Section B **62**, 129 (1949), URL https://doi.org/10.1088/0370-1301/62/2/307.

[50] G. W. Milton and J. R. Willis, Proceedings of the Royal Society A: Mathematical, Physical and Engineering Sciences **463**, 855 (2007).

[51] S. H. Lee and O. B. Wright, Phys. Rev. B **93**, 024302 (2016), URL https://link.aps.org/doi/10.1103/PhysRevB.93.024302.

[52] Y. Bao, M. Rachh, E. Keaveny, L. Greengard, and A. Donev, Journal of Computational Physics **374**, 1094 (2018), ISSN 0021-9991.

[53] M. Minnaert, Philosophical Magazine **16**, 235 (1933), https://doi.org/10.1080/14786443309462277, URL https://doi.org/10.1080/14786443309462277.

[54] T. K. Caughey and M. E. J. O'Kelly, Journal of Applied Mechanics **32**, 583 (1965), ISSN 0021-8936, https://asmedigitalcollection.asme.org/appliedmechanics/article-pdf/32/3/583/5446936/583_1.pdf, URL https://doi.org/10.1115/1.3627262.

[55] A. Lošdorfer Božič and S. Čopar, Phys. Rev. E **99**, 032601 (2019), URL https://link.aps.org/doi/10.1103/PhysRevE.99.032601.

[56] S. Succi, *The Lattice Boltzmann Equation: For Complex States of Flowing Matter* (OUP Oxford, 2018), ISBN 9780192538857, URL https://books.google.si/books?id=uHpVDwAAQBAJ.

[57] C. S. Peskin, Acta Numerica **11**, 479–517 (2002).

[58] P. Ahlrichs and B. Dünweg, The Journal of Chemical Physics **111**, 8225 (1999), https://doi.org/10.1063/1.480156, URL https://doi.org/10.1063/1.480156.

[59] J. Mathews, Journal of the Society for Industrial and Applied Mathematics **10**, 768 (1962), https://doi.org/10.1137/0110059, URL https://doi.org/10.1137/0110059.

[60] F. J. Zerilli, Journal of Mathematical Physics **11**, 2203

(1970), https://doi.org/10.1063/1.1665380, URL `https://doi.org/10.1063/1.1665380`.

[61] K. S. Thorne, Rev. Mod. Phys. **52**, 299 (1980), URL `https://link.aps.org/doi/10.1103/RevModPhys.52.299`.